Electroanalysis of Gallic and Ellagic Acids at a Boron-doped Diamond Electrode Coupled with High-Performance Liquid Chromatography

*Phyllis E. Hayes,[a] Jeremy D. Glennon,[a] and John H.T. Luong [a]**

[a] *Innovative Chromatography Group, Irish Separation Science Cluster (ISSC), School of Chemistry and the Analytical & Biological Chemistry Research Facility (ABCRF), University College Cork, College Road, Cork T12 YN60, Ireland.*

* Email: luongprof@gmail.com

Received: ((will be filled in by the editorial sttaff))
Accepted: ((will be filled in by the editorial sttaff))

Abstract
Electrochemistry of gallic acid (GA) and ellagic acid (EA) was investigated by cyclic voltammetry (CV) using a bare boron-doped diamond (BDD) electrode. CVs indicate that the electro-oxidation of both GA and EA are quasi-reversible processes. High-performance liquid chromatography (HPLC) coupled with a BDD electrode poised at + 1.4 V offers the limit of detection (LOD, S/N = 3) of 60 and 200 nM for GA and EA, respectively. The optimized method was then applied to the detection of both acids in Islay, Highland and Scotch whiskeys, with the highest concentrations found in a 14-year-old Highland whiskey.

Keywords: *Boron-doped diamond electrode. Gallic and ellagic acids. High-performance liquid chromatography. Whiskey.*

DOI: 10.1002/elan.((will be filled in by the editorial sttaff))

1. Introduction

Gallic acid (GA), and particularly its dimer, ellagic acid (EA), are a group of naturally occurring polyphenol antioxidants [1] that have a wide range of biological activities and applications. In brief, GA (3,4,5-trihydroxybenzoic acid) is found in most plants as both free and as part of hydrolyzable tannins [2]. GA is particularly abundant in red wine, green tea, and other processed beverages [3]. It is synthesized from 3-dehydroshikimate by shikimate dehydrogenase to form 3,5-didehydroshikimate, which undergoes tautomerization to form gallate [4]. EA is a dimer of GA, which is also abundant in fruits and vegetables (Scheme 1). Ellagitannin is a more complex version of EA in some fruits but it is converted into EA in the body [5]. This acid with antioxidative and antiviral properties, has been used in food preservation, herbal medicine, and dietary supplements prepared from fruit extracts.

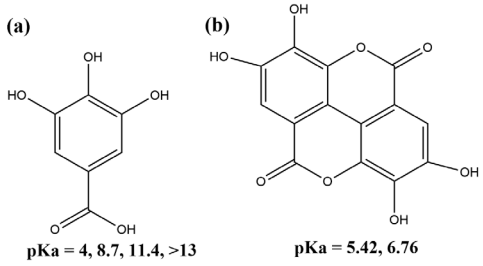

Scheme 1. Chemical structures of GA (a) and EA (b).

EA finds its way into whiskey during the germination of barley, one of the important stages of whiskey production, in which ellagitannin [6] is hydrolyzed to form EA. Worth noting is the use of oak wood casks for the storage of whiskey, brandies, and other alcoholic beverages. During this period, a series of reactions and transfers occur between the wood and the beverage with the level of GA in brandies ranging from 0 to 17.43 mg/L

[7]. The difference in the GA concentrations is due to many factors such as the length of storage, wood type (French oak vs American oak), and the age and life of the barrel (overused and exhausted).

Electroanalysis of GA in food matrices by different electrode materials has been attempted. In brief, a graphite electrode modified with thionine and nickel hexacyanoferrate exhibits a limit of detection (LOD) of 1.66 μM for GA [8]. A glassy carbon electrode (GCE) modified by epinephrine has an LOD of 0.66 μM for GA, compared to 0.28 μM for a GCE modified with silver nanoparticles and delphinidin, a plant pigment [9]. TiO_2 nanoparticles have been used to modify a carbon paste electrode with a comparable LOD of 0.94 μM for this acid [10].

Pertaining to EA, bare platinum, gold, and a GCE has been attempted for electroanalysis and the best response signal is obtained by the GCE [11]. The GCE modified by a cobalt (II) ethylenediamine complex exhibits linearity of 0.1- 929 μM for this acid [12]. The application of this approach focuses on the determination of spiked EA (10-20 μM) in raspberry and strawberry [12]. Of notice is the study of the electroanalytical behavior of GA and EA acid using a screen-printed electrode modified with graphene [13]. Both GA and EA are determined together with other phenols as a single peak to represent the total content of phenolic compounds in cork boiling water. Electroanalysis is a surface dependent method, thus, the reproducibility of the active area of modified electrodes is still problematic.

Analysis of GA and EA is of importance for diversified fields, e.g., medical, biomedical, and pharmaceutical applications. Electrochemical sensors have offered several appealing features, including enhanced detection sensitivity, cost-effectiveness, and ease of fabrication. This study aims to develop a high-performance liquid chromatography (HPLC) technique equipped with a boron-doped diamond (BDD) electrode for rapid co-analysis of GA and EA in whiskeys as a model. HPLC coupled to a BDD electrode provides enhanced selectivity and specificity for phenolic compounds over direct electrochemical detection and HPLC-UV. Electrochemistry of GA and EA on the bare BDD electrode is also investigated in-depth considering this topic has not been attempted. The isolation and characterization of these two acids are of interest to the pharmaceutical, food industry, and other analytical fields. EA is the end product of the degradation of barley tannins and also present in oak wood. Thus, its analysis is useful for the identification of whiskey counterfeits by several analytical methods including gas chromatography equipped with mass spectroscopy [14].

2. 2 Experimental Section

2.1 Chemicals

Phosphoric acid, acetic acid, formic acid, boric acid, ammonium formate, sodium phosphate monobasic, sodium phosphate dibasic, sodium acetate, acetone, sodium hydroxide, ethanol (EtOH), acetonitrile (ACN), dimethylformamide (DMF), α-cyclodextrin (α-CD), 2-hydroxylpropyl β-cyclodextrin (HP-β-CD), sulfated (S-β-CD), GA and EA were purchased from Sigma-Aldrich (Dublin, Ireland). All reagents used were of the analytical grade of the highest purity, and aqueous solutions were prepared in deionized water (Millipore, Ireland). Stock solutions (1 mM) of GA and EA were prepared in ACN and DMF, respectively. Highland, Scotch, and Islay whiskeys were purchased from a local store in Cork, Ireland. Whiskey samples comprising 500 μL of whiskey and 1000 μL of the mobile phase were filtered through an Econofltr Nylon membrane (13 mm, 0.2 μm) before analysis.

2.2 Voltammetric Analysis

Cyclic voltammetry (CV) and square wave voltammetry (SWV) was applied to investigate the electrochemical behavior of GA and EA using a CHI 1040A electrochemical workstation (CH Instrument, Austin, TX). The electrochemical cell consists of the BDD working electrode (B/C ratio in the gaseous phase of 1000 ppm, 3 mm diameter, Windsor Scientific, Slough Berkshire, UK), a silver/silver chloride (Ag/AgCl /3 M KCl) reference electrode (BASi Analytical Instruments, West Layette, IN), and a Pt wire counter electrode (Sigma-Aldrich, Dublin, Ireland). Phosphate buffers at pH 2 and pH 7, and acetate buffer at pH 5, at a concentration of 100 mM and containing 5% EtOH were used as supporting electrolytes. 5% EtOH was used to eliminate the effect of EtOH in whiskey. Before analysis, the BDD electrode was polished with polishing papers (Buehler, UK) and subsequently with alumina (Buehler, UK) until a mirror finish was obtained. The electrode was then sonicated in ACN and deionized water for 5 min and 10 min, respectively. After sonication, the electrode was cleaned by CV between − 1.0 V and + 1.5 V versus Ag/AgCl (3 M KCl) at 100 mV s^{-1} in 0.5 M H_2SO_4 and then in the respective buffers applied for analysis. Between measurements, the electrode was also cleaned with 0.5 M H_2SO_4 for 10 cycles at a scan rate of 100 mV s^{-1} to remove adsorbed species from its surface.

2.3 Apparatus

HPLC with electrochemical detection (ECD) analyses were performed on an Agilent HPLC system (Agilent

1200 LC series) equipped with a binary pump (model G1312B), degasser (model G1379B), autosampler (model G1367D) and a UV diode array detector (model G1315C). Agilent Chemstation was used for instrument control and UV data analysis. ECD was carried out using an Antec Flexcell thin layer flow cell with a cell volume of 0.7 µL (Apex Scientific, Kildare, Ireland). The flow cell consists of a three-electrode configuration with a working BDD (8 mm diameter), a HyREF (Pd/H_2) reference electrode, and carbon loaded polytetrafluoroethylene (PTFE) counter electrode. CHI 660E electrochemical workstation was used for data analysis (CH Instrument, Austin, Texas). Between measurements, the BDD electrode was cleaned by wiping its surface firstly with H_2O then with acetone using MasterTex paper.

2.4 Chromatographic Conditions

Gradient chromatographic separation was performed using an Agilent XDB C_{18} column (4.6 x 150 mm, 5 µm particle size, Apex Scientific, Kildare, Ireland). Mobile phase A was 10 mM formate, pH 3, and mobile phase B was ACN. Gradient elution was performed starting with 2% B followed by a linear increase to 30% B until 3 min. The next linear increase was until 40% B to 5 min followed by re-equilibration from 5 to 8 min with 2% B. The injection volume was 5 µL and the flow rate was set at 1.5 mL/min. The column temperature was set at 25 °C. HPLC-ECD was determined at + 1.4 V in oxidative mode.

2.5 Method Validation

The method was validated for linearity, LODs, and precision (intra-day and inter-day). The linearity of the method was evaluated by linear regression analysis of six standard working solutions. All standards were run in triplicate. LODs were determined by the lowest concentration with a signal-to-noise ratio of 3 (S/N = 3). Intra-day precision was carried out by five repetitive measurements of a mixed standard solution (100 µM) within one day, and inter-day by five repetitive measurements of a mixed standard solution (100 µM) over four days. Precision was expressed as the relative standard deviation (RSD %).

3 Results and Discussion

3.1 Cyclic Voltammetry of Gallic and Ellagic Acids

CVs of GA on the BDD electrode at pH 2 exhibited two irreversible anodic CV waves whereas the reverse scan only had three significantly smaller cathodic peaks (Figure 1a). The significant difference in peak current areas and the large separation in peak potentials indicate that the electro-oxidation of GA is a quasi-reversible process followed by a chemical reaction. The first wave represents the irreversible oxidation of GA to the semiquinone radical cation ($GA^{\bullet+}$) (b) by a single electron transfer process. This unstable radical cation then loses a proton to form four different semiquinone radicals ($GA^{\bullet}$) (c, d1-d3). Further oxidation leads to the formation of the quinone cation (GA^{+}) (e), followed by the deprotonation of the quinone cation (GA^{+}) to complete the overall two-electron process and the final product is an *o*-quinone form (e) as shown in Scheme 2 [15]. The two oxidation peaks diminished noticeably when the electrode was subject to repeated scanning, indicating the formation of electro inactive species on the electrode's surface. Irreversible behavior of GA on the BDD electrode implied the formation of inactive GA species on the electrode surface. The semiquinone radical cation ($GA^{\bullet+}$) also reacted with free GA adsorbed on the electrode with the participation of the COOH or the -OH group. Indeed, the formation of ester and ether linkages between gallate monomers both in solution and in the adsorbed state has been reported [16].

There was a decrease of the peak current and a shift of the peak potential towards more positive potentials for the five repeated CV waves (Figure 1a). This behavior could be attributed to the formation of electro inactive species to block the electrode surface including the possible formation of polygallic acid [17]. The anodic current corresponding to GA oxidation increased linearly with the square root of the scan rate (data not shown) indicating that the oxidation is a diffusion-controlled process at the electrode surface. There was a linear positive shift of the oxidation peak potential E_p (for the two waves) on increasing scan rate (100–1000 mV s^{-1}), confirming the irreversible behavior of the electro-oxidation of GA. As expected from the participation of proton (H^{+}) in the redox step, the two peak potentials were shifted toward less positive values with increasing pH of electrolyte from pH 2 to pH 5 and then pH 7 (Figure 1 b-c). The two peak intensities at pH 5 and pH 7 became less pronounced than those obtained at pH 2 because GA was chemically deprotonated at such high pH media. Such a result was similar to the electrochemical behavior of GA in aqueous solutions at a GCE [15]. Free radicals produced by the oxidation of GA have been described from an electron paramagnetic resonance study [18]. However, GA produces two different radicals as a function of pH and the spectrum of the gallate free radical is a doublet of triplets in the pH range between7-10 [18]. Thus, this evidence supported the electrochemical oxidation pathway for GA as reported in the literature [15].

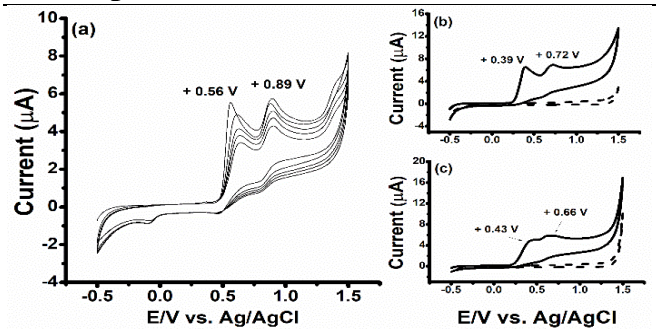

Fig. 1. A representative 5 cycle CV of 100 μM GA at pH 2 (a), CV response in the absence (dashed lines) and presence (solid lines) of 100 μM GA at pH 5 (b) and pH 7 (c) on the BDD electrode vs. Ag/AgCl. Supporting electrolyte: 100 mM phosphate buffer with 5% EtOH at the scan rate of 100 mVs^{-1}.

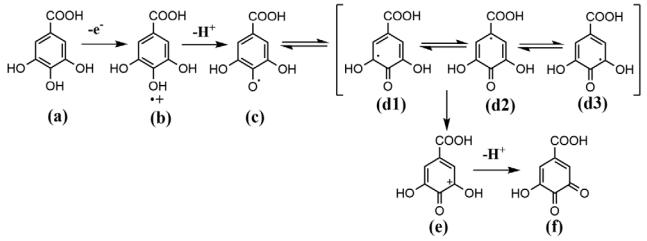

Scheme 2. Electro-oxidation of GA. The process involves the release of two electrons and two H^+, i.e., electrochemistry of GA is pH-dependent. The first step represents irreversible oxidation of GA (a) to the semiquinone radical cation (b). The radical cation (b) then loses a proton to form the semiquinone radical (c, d1-d3). The one-electron oxidation product (d1-d3) is followed by a second irreversible electron transfer to the quinone cation (e). This quinone cation (e) is deprotonated to give the quinone (f) as the final product [15].

At pH 2, the CV of EA exhibited two anodic peaks with the first peak positioned as a shoulder of the second one (Figure 2a). In the reverse scan, two significantly smaller peaks appear, indicating the electro-oxidation of EA was a quasi-reversible process. Having four hydroxyl groups, its electrochemical behavior was significantly affected by pH. In neutral pH, the shoulder developed into a separate peak 2 (Figure 2b). In the reverse scan, two smaller peaks appeared, indicating the electro-oxidation of EA was similar to that of GA, i.e., a quasi-reversible process. Peak 1 was attributed to the formation of EA phenoxyl radical by the release of one electron and one proton (Scheme 3) [19]. A plot of peak potential versus pH gave a slope of close to – 60 mV/pH (data not shown), indicating an equal number of electrons and protons involved in the electrode process. Below pH 4.8, the phenoxyl radical formed in the first oxidation step was stable and underwent a further one-electron, one-proton charge-transfer reaction leading to peak 2 (Scheme 4) [19]. EA, with two carbonyl groups in the molecule, can be reduced at the electrode surface involving two electrons each [20]. A plot of peak current versus square root of the scan rate was linear (data not shown), indicating that EA undergoes a diffusion-controlled process on the electrode surface.

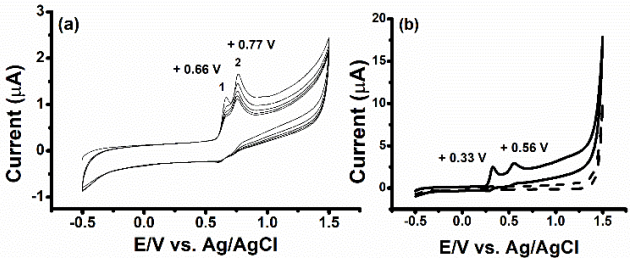

Fig. 2. A representative 5 cycle CV of 100 μM EA at pH 2 (a), CV response in the absence (dashed line) and presence (solid line) of 100 μM EA at pH 7 (b) on the BDD electrode vs. Ag/AgCl. Supporting electrolyte: 100 mM phosphate buffer with 5% EtOH at the scan rate of 100 mVs^{-1}.

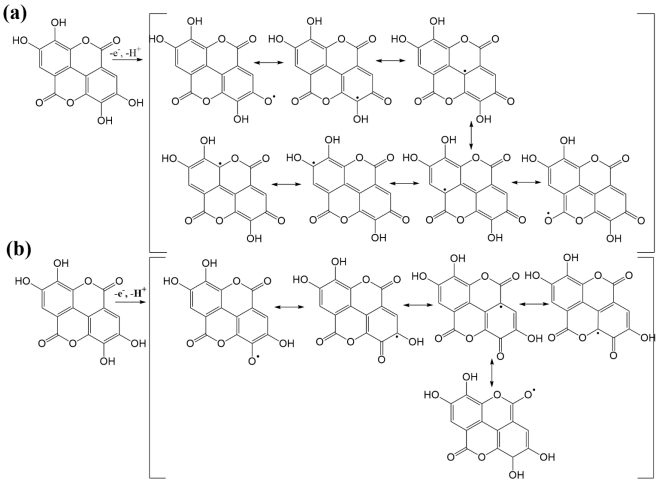

Scheme 3. Two possible electrochemical oxidation pathways of EA to form its corresponding radicals. This first step involves the release of one electron and one H^+ [19].

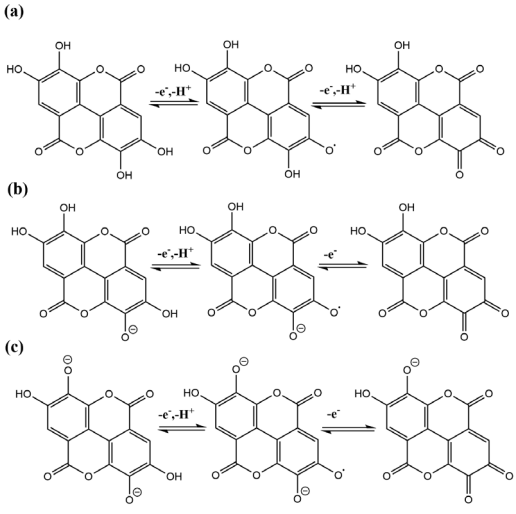

Scheme 4. The formation of different quinones from three different radicals resulted from the electrochemical oxidation of EA. Modified from Ref. [19].

3.2 Square Wave Voltammetry of Gallic and Ellagic Acids

The GA-EA pair was not separated by SWV at three different pHs: 2, 5, and 7 (figure not shown). A series of experiments was then conducted to investigate the presence of α-CD, HP-β-CD, and S-β-CD in the electrolyte (Figure 3). Such cyclodextrins might form different inclusion complexes with GA and EA, and this strategy has been used with some success for the analysis of guaiacol and its derivatives in whiskey [21]. In particular, GA forms an inclusion complex with 2-hydroxylpropyl β-CD to improve the solubility of this acid for the treatment of *Candida albicans* films [22]. In general, a broad peak with a noticeable shoulder was observed with all tested CDs. Peak deconvolution was performed to assign the presence of GA and EA (Figure 3). Therefore, an upstream separation scheme is required to quantify the unknown levels of these two acids.

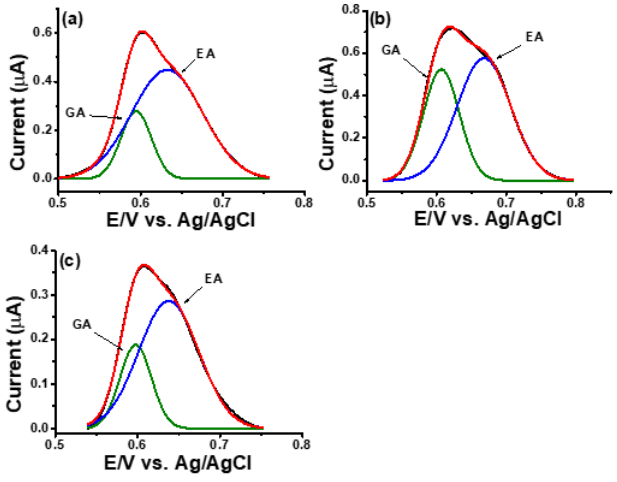

Fig. 3. Resolved SWV of a standard mixture (10 µM GA and 3 µM EA) upon application of peak deconvolution using Origin Pro 8.5.1. Supporting electrolyte: 100 mM phosphate buffer, pH 2 with 5% EtOH containing 1% α-CD (a), 1% S-β-CD (b) and 1% HP-β-CD (c). Detection was achieved on the BDD electrode vs. Ag/AgCl.

3.3 HPLC equipped with the BDD Electrode for Separation and Analysis of Gallic and Ellagic Acids

Isocratic elution was first investigated for the separation of GA and EA. However, due to the large difference in polarity between the analytes, it proved difficult to sufficiently retain GA without high retention and significant peak broadening of EA occurring. Therefore, gradient elution was applied to shorten the run time and provide sufficient retention of the analytes. The separation was achieved in a linear gradient elution profile with a binary mobile-phase mixture of 10 mM formate buffer, pH 3 (A) and ACN (B). The gradient profile involved an initial 2% B, followed by a linear increase to 30% B until 3 min. The next linear increase was until 40% B to 5 min followed by re-equilibration from 5 to 8 min with 2% B. A buffer of pH 3 was chosen as it ensured that GA (lowest pK_a ~ 4.4) was in its unionized form, enabling its increased retention. The flow rate was set at 1.5 mL/min, the maximum allowed flow rate compatible with the ECD system (Figure 4).

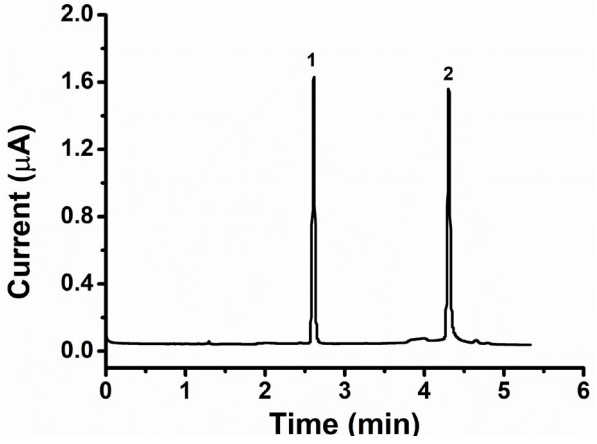

Fig. 4. 50 µM standard mixture of GA (1) and EA (2). Column: Agilent XDB C_{18} (4.6 x 150 mm, 5 µm), mobile phase flow rate: 1.5 mL/min, injection volume: 5 µL, oxidation potential: + 1.4 V on the BDD electrode vs. Pd/H_2.

Experiments were then conducted to determine the optimum detection potential, by establishing the relationship between the applied working electrode potential and detector response for the analytes. The hydrodynamic voltammograms are shown in Figure 5. At + 1.6 V and + 1.8 V, a noticeable increase in background current and baseline drift occured. The baseline noise also increased due to the electro-oxidation of possible impurities present in the mobile phase. The oxidation potential of + 1.4 V provided sufficient sensitivity with low background noise; therefore, it was chosen as the optimum detection potential (Figures 5 and 6).

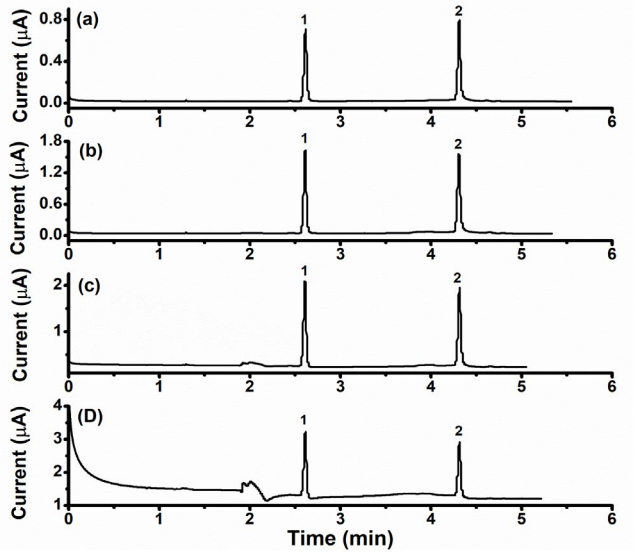

Fig. 5. The effect of oxidation potential on the detection of 100 μM each of GA (1) and EA (2). Oxidation potential: + 1.2 V (a), + 1.4 V (b), + 1.6 V (c) and + 1.8 V (d) on the BDD electrode vs. Pd/H_2. Column: Agilent XDB C_{18} (4.6 x 150 mm, 5 μm), mobile phase flow rate: 1.5 mL/min, injection volume: 5 μL.

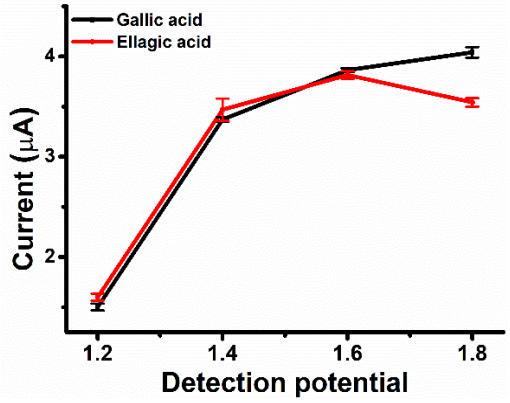

Fig. 6. The plot of oxidation potential (V) versus current (μA) on the BDD electrode vs. Pd/H_2. Column: Agilent C_{18} (4.6 x 150 mm, 5 μm), mobile phase flow rate: 1.5 mL/min, injection volume: 5 μL.

3.4 Analytical Performance for Analysis of Gallic and Ellagic Acids in Whiskey

Analytical parameters such as linearity of calibration curves and LODs were determined for ellagic and gallic acids (Table 1). Calibration curves were evaluated based on the relationship between the concentrations and the corresponding peak areas of the acids. All measurements were performed in triplicate with linearity from 1 to 30 μM. Calibration curves and plots are presented in Figure 7. The LODs of GA and EA were 60 and 200 nM, respectively, considerably lower than LODs determined with UV detection under the same separation conditions (Table 2), and also lower than previously reported LC-UV methods [23–25]. Intra-day and inter-day precision were in the range of 0.23 – 0.47 % and 0.64 – 1.02 % RSD, respectively.

Table 1. Linear regression parameters of calibration curves for gallic and ellagic acids detected with HPLC-ECD at + 1.4 V.

Analyte	Linear range (μM)	Linear regression equation	Correlation coefficient (R^2)
Gallic acid	1-30	$I = 6.320 \times 10^{-8} C + 2.894 \times 10^{-10}$	0.999
Ellagic acid	1-30	$I = 4.248 \times 10^{-8} C - 6.771 \times 10^{-9}$	0.995

Table 2. Comparison of LODs obtained with ECD and UV detection.

Analyte	LOD[a] HPLC-ECD	LOD[b] HPLC-UV
Gallic acid	60 nM	1 μM
Ellagic acid	200 nM	1.5 μM

[a] LOD (*S/N* = *3*) at + 1.4 V.

[b] LOD (*S/N* = *3*) at 272 nm.

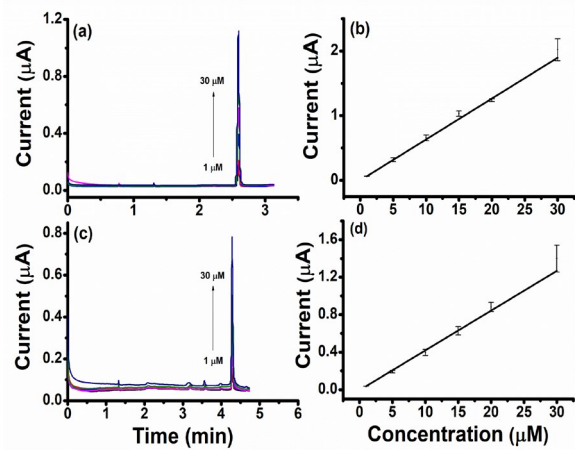

Fig. 7. The calibration curve (a) and plot (b) of GA, and the calibration curve (c) and plot (d) of EA. Column: Agilent XDB C_{18} (4.6 x 150 mm, 5 μm), mobile phase flow rate: 1.5 mL/min, injection volume: 5 μL, oxidation potential: + 1.4 V on the BDD electrode vs. Pd/H_2.

3.5 Detection of Gallic and Ellagic Acids in Whiskey Samples

The optimal HPLC-ECD method was then applied to determine the concentrations of GA and its derivative, EA in three whiskey samples (Figure 8). Highland (14-year-old) whiskey contains higher concentrations than

both Islay (10-year-old) and Scotch (exact age unknown) whiskeys (Table 3). This is not unexpected, as the concentrations of gallic and ellagic acids in whiskey are proven to increase with an increase in maturation age [26]. % RSD values of 1.4 – 3.19 % and 1.31 – 2.85 % for the peak areas of GA and EA, respectively, in the whiskeys (n=3) indicate high reliability in the concentrations of the acids determined. Concentrations of 1 – 35 µM and 8 – 99 µM of GA and EA, respectively, are reported in unidentified Scotch whiskeys [27]. EA was also identified as the predominant phenolic constituent in both single-malt Scotch (~33 µM) and blended Scotch (~17 µM) [28] whiskey. The presence of other peaks in the whiskey samples (Figure 8) encompassing several phenolic compounds, has been identified and reported by HPLC equipped with a BDD electrode [29].

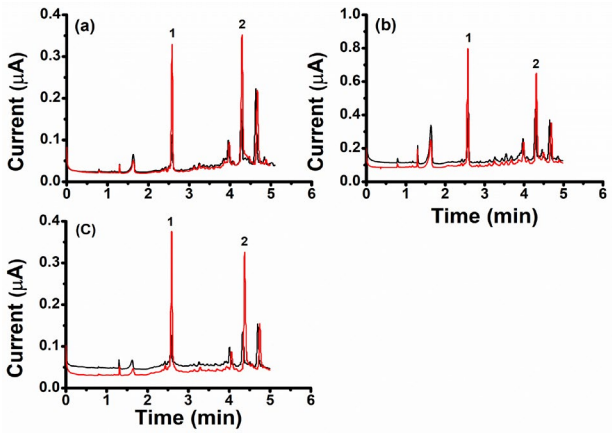

Fig. 8. HPLC-ECD chromatograms of Islay whiskey (a), Highland whiskey (b), and Scotch whiskey (c). Whiskey (black line) and spiked with 10 µM each of GA (1) and EA (2) (red line). Column: Agilent XDB C_{18} (4.6 x 150 mm, 5 µm), mobile phase flow rate: 1.5 mL/min, injection volume: 5 µL, oxidation potential: + 1.4 V on the BDD electrode vs. Pd/H_2.

Table 3. The concentration of gallic and ellagic acids in three whiskey samples (n = 3).

Analyte	Islay (µM)	Highland (µM)	Scotch (µM)
Gallic acid	7.98 ± 0.17	33.77 ± 1.6	5.86 ± 0.41
Ellagic acid	25.10 ± 1.15	55.41 ± 0.7	15.85 1.24

4 Conclusions

Electro-oxidation of EA and GA at low pH produces two anodic peaks, with two smaller cathodic peaks for EA and three smaller cathodic peaks for GA, indicating quasi-reversible processes. At high pH, there was a noticeable reduction in peak intensities as a result of the chemical deprotonation of these two acids. HPLC-BDD was successfully applied for the detection of GA and EA in Islay, Highland, and Scotch whiskeys. GA and EA are identified as possible discriminants for single malt whiskey [14]. Higher concentrations of both acids were found in Highland whiskey due to a longer period of maturation of this whiskey, compared to its counterparts. As GA and EA are naturally occurring polyphenols, the nanomolar detection achieved with LC-BDD may prove attractive towards their detection in the food and medical fields. GA has also been used extensively in the manufacturing of paper, ink dye, and tanning [30] whereas its dimer is used in food preservation [31]. Besides HPLC, capillary electrophoresis (CE) also serves as an upstream separation scheme to separate EA from GA, particularly in the presence of cyclodextrins and their derivatives [32]. Both HPLC and CE are miniaturized and equipped with the BDD electrode towards the fabrication of portable devices for diversified analytical fields.

5 Acknowledgments

JDG thanks the Science Foundation Ireland (08/SRC/B1412) for research funding of the Irish Separation Science Cluster (ISSC) under the Strategic Research Cluster Programme. JDG acknowledges support by Enterprise Ireland (CF-2017-0759-P). PEH acknowledges support by the Irish Research Council (IRC/EPSPG/2015/113).

6 References

[1] F. Shahidi, J. D. Yeo, *Int. J. Mol. Sci.* **2018**, *19*, 1–16.

[2] J. Dai, R. J. Mumper, *Molecules* **2010**, *15*, 7313–7352.

[3] C. Cabrera, R. Artacho, R. Giménez, *J. Am. Coll. Nutr.* **2006**, *25*, 79–99.

[4] R. M. Muir, A. M. Ibáñez, S. L. Uratsu, E. S. Ingham, C. A. Leslie, G. H. McGranahan, N. Batra, S. Goyal, J. Joseph, E. D. Jemmis, et al., *Plant Mol. Biol.* **2011**, *75*, 555–565.

[5] M. Sharma, L. Li, J. Celver, C. Killian, A. Kovoor, N. P. Seeram, *J. Agric. Food Chem.* **2010**, *58*, 3965–3969.

[6] N. Vivas, N. Vivas de Gaulejac, C. Vitry, C. Mouche, N. Kahn, M. F. Nonier-Bourden, C. Absalon, *J. Inst. Brew.* **2013**, *119*, 116–125.

[7] M. Cabrera, C., Mejia-Lopez, H., Navarro-Alarcon, M., Olalla, *Cienc. Tecnol. Aliment* **2000**, *3*, 13–20.

[8] N. S. Sangeetha, S. S. Narayanan, *Anal. Chim. Acta* **2014**, *828*, 34–45.

[9] M. Ghaani, N. Nasirizadeh, S. A. Yasini Ardakani, F. Z. Mehrjardi, M. Scampicchio, S. Farris, *Anal. Methods* **2016**, *8*, 1103–1110.

[10] J. Tashkhourian, S. F. N. Ana, S. Hashemnia, M. R. Hormozi-Nezhad, *J. Solid State Electrochem.* **2013**, *17*, 157–165.
[11] V.-A. Mitrancă, M. C. Cheregi, I. G. David, *Proceedings* **2019**, *29*, 35.
[12] S. Sakthinathan, T. Kokulnathan, S. M. Chen, T. W. Chen, T. W. Tseng, X. Liu, W. C. Liao, *Int. J. Electrochem. Sci.* **2017**, *12*, 6829–6841.
[13] A. Guiberteau-Cabanillas, B. Godoy-Cancho, E. Bernalte, M. Tena-Villares, C. Guiberteau-Cabanillas, M. A. Martínez-Cañas, *Electroanalysis* **2015**, *27*, 177–184.
[14] M. Stupak, I. Goodall, M. Tomaniova, J. Pulkrabova, J. Hajslova, *Anal. Chim. Acta* **2018**, *1042*, 60–70.
[15] R. Abdel-Hamid, E. F. Newair, *J. Electroanal. Chem.* **2011**, *657*, 107–112.
[16] I. Y. Tóth, M. Szekeres, R. Turcu, S. Sáringer, E. Illés, D. Nesztor, E. Tombácz, *Langmuir* **2014**, *30*, 15451–15461.
[17] A. Romero-Montero, A. Tecante, R. García-Arrazola, C. Montiel, L. J. Del Valle, J. Puiggalí, M. Gimeno, *RSC Adv.* **2017**, *7*, 17660–17669.
[18] A. C. Eslami, W. Pasanphan, B. A. Wagner, G. R. Buettner, *Chem. Cent. J.* **2010**, *4*, 1–4.
[19] A. Z. Simić, T. Ž. Verbić, M. N. Sentić, M. P. Vojić, I. O. Juranić, D. D. Manojlović, *Monatshefte fur Chemie* **2013**, *144*, 121–128.
[20] K. Thakur, K. S. Pitre, *J. Chinese Chem. Soc.* **2008**, *55*, 143–146.
[21] P. E. Hayes, J. D. Glennon, A. Buzid, J. H. T. Luong, *Electroanalysis* **2020**, *32*, 119–127.
[22] G. R. Teodoro, A. V. L. Gontijo, A. C. Borges, M. H. Tanaka, G. D. M. G. Lima, M. J. Salvador, C. Y. Koga-Ito, *PLoS One* **2017**, *12*, 1–15.
[23] F. H. A. Fernandes, R. S. A. de Batista, F. D. de Medeiros, F. S. Santos, A. C. D. Medeiros, *Brazilian J. Pharmacogn.* **2015**, *25*, 208–211.
[24] I. S. Shalavadi, M.H., Chandrashekhar, V.M., Muchchandi, *Int. J. Green Pharm.* **2019**, *13*, 236–241.
[25] P. I. D. Assunção, E. C. Da Conceição, L. L. Borges, J. A. M. De Paula, *Evidence-based Complement. Altern. Med.* **2017**, *2017*, 1–9.
[26] H. Koga, K., Taguchi, A., Koshimizu, S., Suwa, Y., Yamada, Y., Shirasaka, N., Yoshizumi, *J. Food Sci.* **2007**, *72*, 212–217.
[27] S. E. R. Bukovsky-Reyes, L. E. Lowe, W. M. Brandon, J. E. Owens, *J. Inst. Brew.* **2018**, *124*, 291–299.
[28] D. M. Goldberg, B. Hoffman, J. Yang, G. J. Soleas, *J. Agric. Food Chem.* **1999**, *47*, 3978–3985.
[29] P. E. Hayes, J. H. T. Luong, E. S. Gilchrist, A. Buzid, J. D. Glennon. *J. Chrom. A* **2020**, *1612*, 460649.
[30] A. D. Covington, *Chem. Soc. Rev*. **1997**, *26*:111-126.
[31] A. S. Kumar, Y. M. Ji, S. Sornambikai, P. Y. Chen, Y. Shih, *Int. J. Electrochem. Sci*. **2011**, *6*, 5344-5356.
[32] R.S. Brown, J.H.T. Luong, O.H.J. Szolar, A. Halasz, J. Hawari. *Anal. Chem*. **1996**, *68*, 287-292.

TOC